# $CO_2$ Absorption on $Na_2ZrO_3$: A Kinetic Analysis of the Chemisorption and Diffusion Processes

**Itzel Alcérreca-Corte, Esteban Fregoso-Israel, and Heriberto Pfeiffer***

*Instituto de Investigaciones en Materiales, Universidad Nacional Autónoma de México, Circuito Exterior s/n CU, Del. Coyoacán, CP 04510, México DF, Mexico*

*Received: October 30, 2007; In Final Form: February 14, 2008*

The kinetics analysis of carbon dioxide ($CO_2$) chemisorption on sodium zirconate ($Na_2ZrO_3$), which implies a sodium diffusion process, was investigated. Initially, $Na_2ZrO_3$ was analyzed by X-ray diffraction, scanning electron microscopy, and $N_2$ adsorption, to characterize the material. Finally, the material was thermally analyzed under a $CO_2$ flux. Later, different isothermal experiments were performed under a $CO_2$ flux to study kinetically the $CO_2$ chemisorption on $Na_2ZrO_3$. Results showed that there is a sintering effect of the sample during the heating process. This effect produced, at low temperatures, a decrease in the $CO_2$ chemisorption efficiency. However, at high temperatures, once the sodium diffusion was activated, the sintering effect did not interfere with the $CO_2$ chemisorption process. Modeling the $CO_2$ chemisorption on $Na_2ZrO_3$ (in terms of a double process: chemisorption and sodium diffusion) allowed us to estimate the activation energy for these processes, 33 866 J/mol (chemisorption) and 48 009 J/mol (diffusion), which demonstrated that the diffusion process is the limiting step.

## Introduction

Greenhouse gases are components of the atmosphere that contribute to the greenhouse effect, which is a natural process that is necessary for life to exist on Earth. However, in the last few decades, the increment of these gases, produced from human activities, has produced an overwarming of the Earth. Among these gases, carbon dioxide ($CO_2$) is one of the most important because it is produced due to the burning of fossil fuels.[1−5]

One of the possible solutions proposed for the reduction of $CO_2$, emitted to the atmosphere, is to trap it.[6] In this capacity, different kinds of materials have been proposed as $CO_2$ captors, for example, polymeric membranes, zeolites, hydrocalcite-like materials, and different oxides.[7−11] Additionally, since 1998, the use of different alkaline ceramics for trapping $CO_2$ has been proposed (i.e., $Li_2ZrO_3$, $Li_6Zr_2O_7$, $Li_4SiO_4$, $Li_2O$, $Na_2ZrO_3$, and different solid solutions of them).[1,6,12−24] Among the alkaline zirconates, sodium metazirconate ($Na_2ZrO_3$) seems to present much better properties, as a $CO_2$ captor, than lithium zirconates.[25−27] $Na_2ZrO_3$ has a lamellar structure, where sodium atoms are located among the $(ZrO_3)^{2-}$ layers, which allows for sodium diffusion. The mechanism for $CO_2$ absorption (chemisorption) on $Na_2ZrO_3$ and alkaline oxide ceramics in general has been proposed.[13] First, the surface of the alkaline ceramic particles reacts with $CO_2$, producing an external shell of carbonate. Later, once the carbonate external layer is completely produced, sodium atoms, in this case, have to diffuse throughout this external carbonate shell to reach the surface and be able to react with the $CO_2$. For $Na_2ZrO_3$, the total process can be simply described by reaction 1

$$Na_2ZrO_3 + CO_2 \rightarrow Na_2CO_3 + ZrO_2 \qquad (1)$$

where the maximum theoretical $CO_2$ absorption should correspond to an increase of weight equal to 23.75 wt %. Hence, the reaction is controlled by two different processes: $CO_2$ absorption over the surface of the $Na_2ZrO_3$ particles and sodium diffusion.

Although $CO_2$ absorption over $Na_2ZrO_3$ already has been reported,[25−27] there is not any kinetic information of this process. It has only been reported qualitatively that $CO_2$ chemisorption on $Na_2ZrO_3$ takes place approximately between 120 and 800 °C and that the desorption process occurs at higher temperatures[27] or can be produced not thermically but chemically. Therefore, the aim of this work was to study systematically the kinetic process of $CO_2$ absorption on $Na_2ZrO_3$ in a wide range of temperatures to obtain different kinetic parameters of the whole process.

## Experimental Procedures

Sodium metazirconate ($Na_2ZrO_3$) was synthesized by a solid-state method. It was produced from a mechanical mixture of zirconium oxide ($ZrO_2$, Aldrich) and sodium carbonate ($Na_2CO_3$, Aldrich). The reaction was performed using stoichiometric Na/Zr molar ratios (2:1) to obtain $Na_2ZrO_3$. Then, the powder mixture was heat-treated at 900 °C for 4 h.

The produced powders were characterized, before and after the $CO_2$ sorption processes, by different techniques such as powder X-ray diffraction (XRD), scanning electron microscopy (SEM), $N_2$ adsorption (BET method), and thermogravimetric analysis (TGA). The XRD patterns were obtained with a Bruker AXS Avance D8 diffractometer coupled to a Cu anode X-ray tube. The K$\alpha$1 wavelength was selected with a diffracted beam monochromator, and compounds were identified conventionally using the JCPDS database. SEM (Stereoscan 440, Leica-Cambridge) was used to determine the particle size and morphology of the materials before and after the $CO_2$ sorption process. The samples were covered with gold to avoid a lack of electrical conductivity. Surface area analyses were performed on ASAP 2020 Micromeritics equipment. The $N_2$ adsorption isotherms were determined at 77 K by volumetric adsorption.

* Corresponding author. Tel.: +52 (55) 5622 4627; fax: +52 (55) 5616 1371; e-mail: pfeiffer@iim.unam.mx.

10.1021/jp710475g CCC: $40.75 
Published on Web 04/03/2008

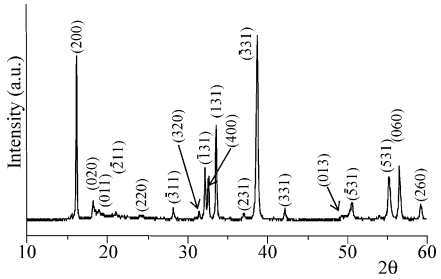


**Figure 1.** XRD pattern of $Na_2ZrO_3$ synthesized by the solid-state method. The composition of the sample was compared and indexed according to JCPDS file no. 35-0770.

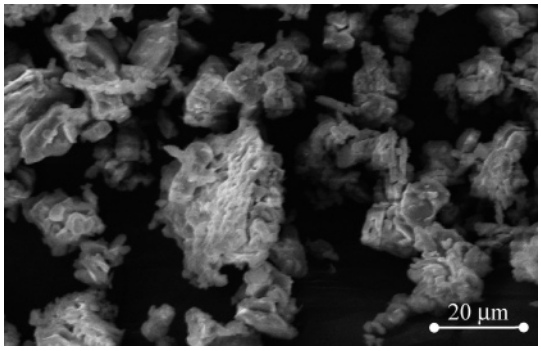


**Figure 2.** SEM image of the $Na_2ZrO_3$ sample prepared by the solid-state method.

Before the $N_2$ adsorption process, samples were outgassed at 200 °C for 12 h. Surface areas were calculated with the BET equation, and pore diameter values were calculated with the BJH method. Finally, different thermal analyses were performed in high-resolution TGA 2950 thermogravimetric analyzer equipment from TA Instruments. First, the sample was heat-treated, with a heating rate of 5 °C $min^{-1}$, from room temperature to 1000 °C under $CO_2$ flux. Additionally, another set of samples was analyzed isothermically under an atmosphere of $CO_2$, at 150, 200, 250, 300, 550, 600, 650, and 700 °C for 5 h.

## Results and Discussion

**Characterization of the Sample.** To establish the purity of the $Na_2ZrO_3$ sample, it was analyzed by XRD. Figure 1 shows the XRD pattern of the sample after thermal treatment at 900 °C for 4 h. As can be seen, the diffraction pattern perfectly fits to the JCPDS file 35-0770, which corresponds to $Na_2ZrO_3$ with a monoclinic structure. Therefore, $Na_2ZrO_3$ was obtained without the presence of any impurity, at least at the XRD detection level.

The morphology and particle size of this sample were analyzed by SEM (Figure 2). The particles presented a dense polyhedral morphology, with an average particle size of about 1 $\mu$m. These particles produced large agglomerates of around 20−25 $\mu$m. The dense morphology was corroborated by the surface analysis. Figure 3 shows the nitrogen adsorption−desorption isotherm of the $Na_2ZrO_3$ sample. The isotherm was of type III, exhibiting a very narrow H3-type hysteresis loop, according to the IUPAC classification. This behavior corresponds to nonporous dense aggregate particles. In fact, the surface area obtained was very small, only 2.06 $m^2/g$, and the pore diameter value could not be determined.

**Kinetic Analysis of $CO_2$ Absorption.** Once $Na_2ZrO_3$ was characterized, the material was thermally analyzed under a $CO_2$ flux (Figure 4). $Na_2ZrO_3$ presented a high $CO_2$ absorption. $Na_2ZrO_3$ increased its weight by about 20.8 wt % in two different processes, which is in good agreement with previous reports.[25,27] First, the thermogram shows an increase of weight (11.4 wt %) between 20 and 250 °C. This process has been associated to $CO_2$ chemisorption mainly produced on the surface of the $Na_2ZrO_3$ particles. At this point, a thin $Na_2CO_3$ shell should be produced over the surface of the $Na_2ZrO_3$ particles. This was confirmed in this work by analyzing by XRD the products after $CO_2$ absorption and after the isothermal analysis, where a mixture of $Na_2ZrO_3$, $ZrO_2$, and $Na_2CO_3$ was found for all the temperatures in the analysis (data not shown). Coming back to the dynamic thermogram experiment (Figure 4), after the first increase in weight, there was a lag period within which the weight of the sample was essentially invariant (250−370 °C). This could be explained by saturation of $Na_2ZrO_3$ surface particles as $Na_2CO_3$, which inhibits the continuation of the reaction. Later, once sodium diffusion was activated, the weight increased again up to 20.8 wt % between 420 and 740 °C. This second increment of weight was caused by the reactivation of the $CO_2$ absorption process, produced by sodium diffusion, from the core to the surface of the particles.

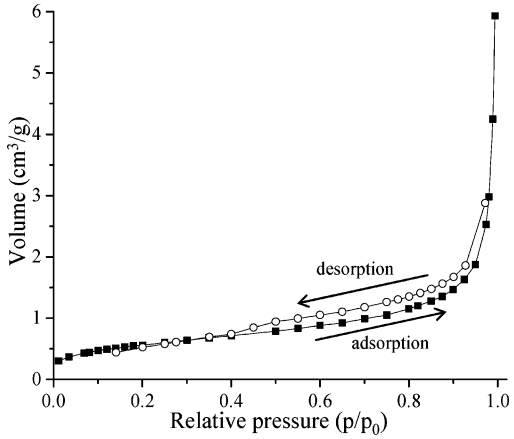


**Figure 3.** Nitrogen isotherm (adsorption/desorption) of the $Na_2ZrO_3$ sample.

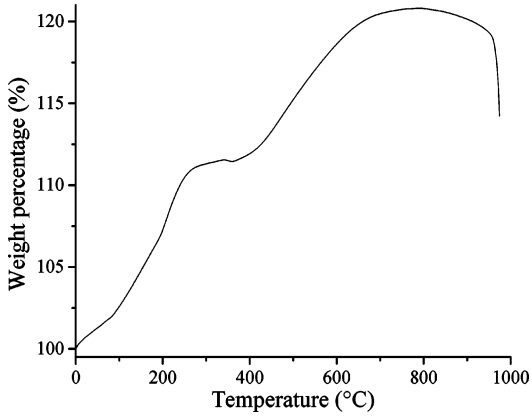


**Figure 4.** TGA curve of $Na_2ZrO_3$ analyzed under a flux of $CO_2$.

On the basis of these results, $Na_2ZrO_3$ was analyzed isothermically at different temperatures, to obtain kinetic information. Figure 5 shows the isothermal graphs of $Na_2ZrO_3$ at different temperatures. At high temperatures (550−700 °C), as was expected, $CO_2$ chemisorption was very fast. Additionally, at 700 °C, the sample presented a narrow $CO_2$ desorption process, and it is analyzed and discussed next. Nevertheless, at low temperatures (150−300 °C), the behavior observed was atypical. The isotherm at 150 °C showed an exponential behavior, which had not reached the plateau after 5 h. In this case, the absorption was equal to 17 wt % (efficiency of 70%). At this temperature,

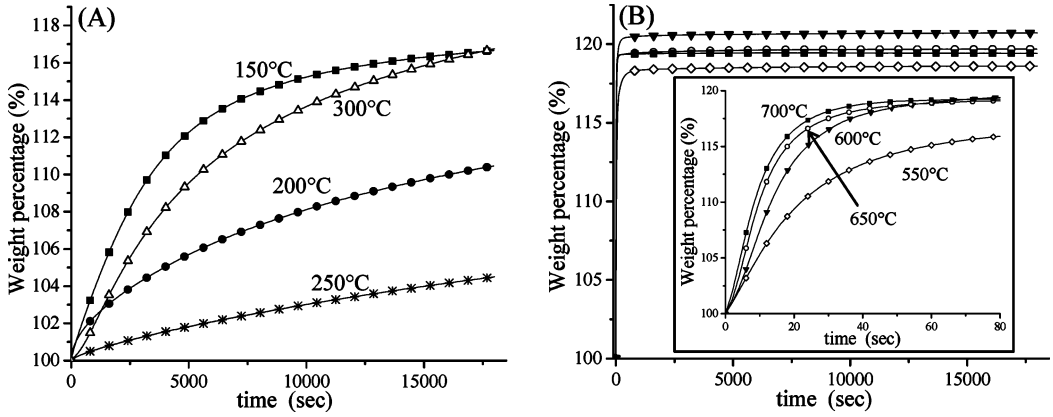


**Figure 5.** Isotherms of $CO_2$ sorption on $Na_2ZrO_3$ at different temperatures into a flux of $CO_2$. (A) Isotherms obtained between 150 and 300 °C. (B) Isotherms obtained between 550 and 700 °C, where the inset graph only shows the first 80 s of these isothermal experiments.

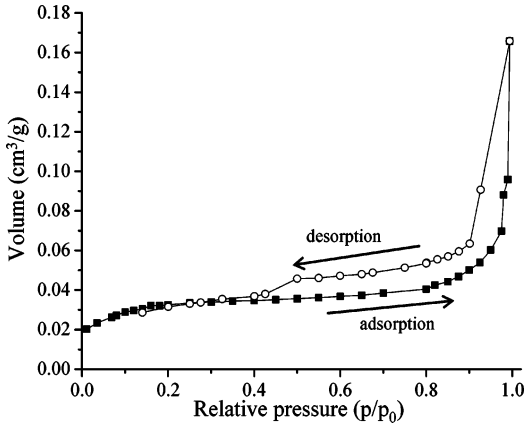


**Figure 6.** Nitrogen isotherm (adsorption/desorption) of the $Na_2ZrO_3$ sample after thermal shock treatment.

150 °C, sodium diffusion should occur due to the efficiency obtained, but it must be significantly slow, in comparison to the isotherms performed at high temperatures.

At 200 °C, although the sample presented the same exponential behavior, $CO_2$ absorption was slower than that at 150 °C (weight increase was 10 wt %). The same behavior, but more drastic, was observed at 250 °C. At this temperature, the absorption was only 4 wt % after 5 h. One possible explanation for this behavior could be associated with the thermal shock produced on the samples during the heating process (100 °C/min) before the isothermal processes. If that were the case, the sample might have sintered, and therefore, its surface area decreased. If this was the case, although the sintering effect must occur before $CO_2$ absorption took place, it may inhibit $CO_2$ absorption partially due to the reduction of the surface area. To prove this hypothesis, one sample was thermally heated from room temperature to 250 °C at a rate of 250 °C/min, into the thermogravimetric furnace, using a flux of nitrogen. After thermal treatment, the sample was analyzed by XRD, SEM, and $N_2$ adsorption.

Although the composition and morphology of this sintered material (determined by XRD and SEM, respectively, data not shown) did not present any significant variation (it stayed as $Na_2ZrO_3$), $N_2$ adsorption did present slight differences (Figure 6). The isotherm was of type III again, but this sample presented a higher hysteresis, which suggested the presence of some kind of porosity. The sample presented a very similar surface area (2.63 $m^2/g$), but in this case, the pore size could be determined: 46.3850 Å. The formation of pores was greater than that of the original sample, which in fact did not show the presence of porosity. The formation of this porosity can be associated with a sintering effect. Therefore, when the sample was heated, very quickly at 150, 200, and 250 °C, the powder sintered, and this explains as to why the $CO_2$ absorption rate diminished or became slower, due to the formation of pores, which limited the $CO_2$ flux and contact with the $Na_2ZrO_3$ surface, decreasing the reaction rate. Additionally, another factor that limited the reaction was the slow sodium diffusion produced at these low temperatures. In this sense, there is something else that must be mentioned. Isothermal analyses performed previously for $CO_2$ capture on alkaline ceramics only have been presented at high temperatures ($T \geq 400$ °C). In this case, the isotherms detected the influence of the sintering effect only in those isotherms performed at much lower temperatures. Hence, this could explain as to why this phenomenon has not been observed previously, or at least reported, because at high temperatures, the alkaline elemental diffusion is activated, and then the sintering effect becomes negligible. Another option could be that the sintering effect was not present on those ceramics.

Finally, in the isotherm performed at 300 °C, the total weight gain began to increase again, and after 5 h, the quantity of $CO_2$ absorbed was the same as that at 150 °C: 17 wt %. Therefore, although the material must be sintered as well, the sodium diffusion should be slightly more activated, allowing a higher $CO_2$ absorption. This effect was confirmed on the isotherms obtained at high temperatures, where the sintering effect was not observed. In those samples, the absorption was very fast; actually, the exponential curves reached their plateau in just a few minutes (see Figure 5). In those cases, the sodium diffusion must be highly activated, and thus, the surface area is not a limitation for $CO_2$ absorption.

Although the isotherms presented the previously mentioned differences, all of them fitted to a double exponential model

$$y = A \exp^{-k_1 x} + B \exp^{-k_2 x} + C \qquad (2)$$

where $y$ represents the weight percentage of $CO_2$ absorbed, $x$ is the time, $k_1$ and $k_2$ are the exponential constants, and $A$, $B$, and $C$ are the pre-exponential factors. As the experimental results fitted to a double exponential, it means that there are two different processes taking place. Actually, this already has been reported. There is a chemisorption process over the surface of the particles, and once the sodium carbonate shell is produced, the second process begins, sodium diffusion, from the core of the particles to the surface to reactivate the chemisorption process. Similar results have been found for $CO_2$ absorption

**TABLE 1: Kinetic Parameters Obtained from Isotherms of $Na_2ZrO_3$ Fitted to a Double Exponential Model**

| temp (°C) | $k_1$ (1/s) | $k_2$ (1/s) | *A* | *B* | *C* | $R^2$ |
|---|---|---|---|---|---|---|
| 150 | $3.8 \times 10^{-4}$ | $1.7 \times 10^{-4}$ | −9.0306 | −8.0237 | 116.946 | 0.99976 |
| 200 | 0.00116 | $8 \times 10^{-5}$ | −1.4345 | −10.8466 | 112.776 | 0.99986 |
| 250 | 0.003 | $5 \times 10^{-5}$ | −0.3311 | −7.5103 | 107.802 | 0.99985 |
| 300 | 0.0085 | $1.6 \times 10^{-4}$ | −0.5367 | −17.4827 | 117.482 | 0.99906 |
| 550 | 0.04432 | 0.00479 | −15.9246 | −2.8543 | 118.428 | 0.99873 |
| 600 | 0.06141 | 0.00552 | −20.7269 | −1.306 | 120.560 | 0.99631 |
| 650 | 0.08559 | 0.006 | −20.3091 | −0.6329 | 119.506 | 0.99409 |
| 700 | 0.0959 | 0.00695 | −20.2634 | −0.15113 | 119.369 | 0.99774 |

over different alkaline ceramics.[13,15] The $k_1$ and $k_2$ constant values obtained at each temperature are presented in Table 1.

Seeing Table 1, the first result that can be seen is that the $k_1$ (chemisorption) values are 1 order of magnitude higher than those of $k_2$ (diffusion), which means that the limiting step of the total process is the sodium diffusion. Furthermore, the first three $k_2$ values do not follow an increasing trend, as all the other data, and as could be expected. This was explained already due to the sintering effect suffered by the $Na_2ZrO_3$ particles. Nonetheless, this effect was not observed on the $k_1$ values. It seems as if the chemisorption process is independent of the sintering effect.

If both processes, chemisorption ($k_1$) and sodium diffusion ($k_2$), follow a linear trend, as a function of temperature, the gradients of these best fit lines should fit an Arrhenius-type behavior

$$D = D_0 \exp^{(-E_a/RT)} \tag{3}$$

where $D_0$ is the reaction rate constant, $E_a$ is the activation energy of the surface reaction or the diffusion process, $R$ is the gas constant, and $T$ is the absolute temperature. These results are presented in Figure 7. For the chemisorption process, the curve clearly shows a linear trend. Therefore, the $E_a$ of this process, $CO_2$ absorption on $Na_2ZrO_3$, could be calculated: 33 866 J/mol. Nevertheless, the diffusion data presented a more complex behavior. At the lowest temperatures (first three data, 150, 250, and 250 °C), it might be interpreted as a negative activation energy. However, as was explained previously, in those data, the sintering effect prevailed over the diffusion process, which explains this behavior. At higher temperatures, a linear trend can be seen, but with two different slopes. First, with the three data points between 250 and 550 °C, although the diffusion process must prevail, there should be a negative contribution of the sintering effect. Finally, at high temperatures (550−700 °C), the sintering effect should not interfere with the diffusion process. Hence, the $E_a$ for this process was only measured using the high-temperature values, and it was equal to 48 009 J/mol. As could be expected, the $E_a$ value for the diffusion process was higher than that for the chemisorption process, it being the limiting step.

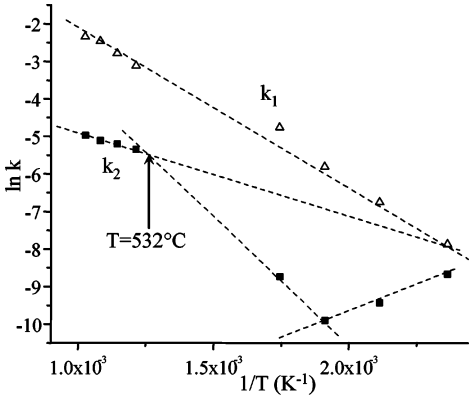


**Figure 7.** Arrhenius-type plots of ln $k$ vs $1/T$, for the two different processes, chemisorption ($k_1$) and diffusion ($k_2$). The arrow shows the point at which the two different linear trends cross, for the diffusion process, which indicates the temperature where the sintering effect stops giving a negative contribution to the sodium diffusion (532 °C).

Two other results are illustrated in Figure 7. First, the crossover of the two linear trends for the diffusion process should correspond to the critical temperature where the sintering effect stops giving a negative contribution to the sodium diffusion. This temperature was equal to 532 °C. Second, taking into account only the chemisorption and diffusion processes, the temperature where these two linear trends crossed (around 150 °C) theoretically indicates the temperature where the diffusion becomes faster than chemisorption. In other words, at lower temperatures than 150 °C, the diffusion should be faster than the chemisorption process. Of course, it cannot be corroborated experimentally because diffusion is measured indirectly through $CO_2$ absorption.

Figure 8 shows the extrapolation of the double exponential model to infinite time for $CO_2$ absorption at different temperatures. As was described already in previous sections, the $CO_2$ absorption capacity decreased between 150 and 250 °C, due to the diminishment of the surface area produced by the sintering effect. This trend corroborates the results obtained previously, where the $Na_2ZrO_3$ sintering effect produced decreases in the surface area, which interfere with $CO_2$ absorption at low temperatures. Conversely, at higher temperatures than 250 °C, two different behaviors can be described. First, $CO_2$ absorption increased as a function of temperature from 250 °C to about 400 °C, and then $CO_2$ absorption was constant (Figure 8, dashed line), reaching an 85% efficiency. However, a second possible explanation could be inferred. In this second option, no statistical error should be assumed, and then the best $CO_2$ absorption is presented at 600 °C, while at 650 and 700 °C, $CO_2$ absorption decreased appreciably. The attenuation of $CO_2$ absorption at high temperatures might be associated with the $CO_2$ absorption/desorption equilibrium. This equilibrium is not present at lower temperatures because there may not be a desorption process. In

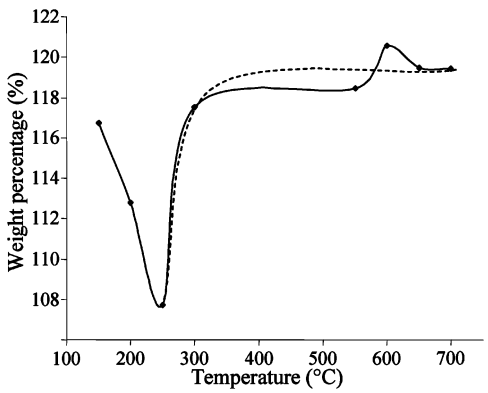


**Figure 8.** Possible tendencies for $CO_2$ saturation values at different temperatures, obtained by the extrapolation of the double exponential model fit to infinite time.

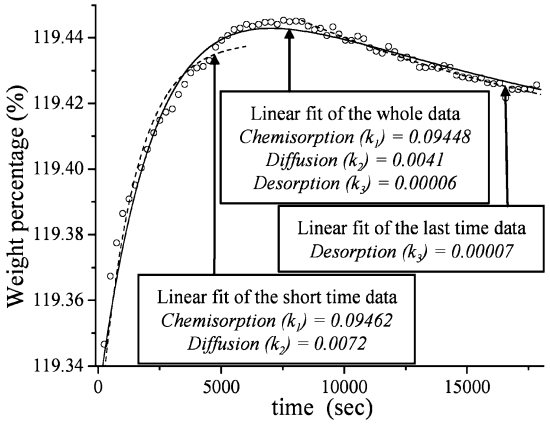


**Figure 9.** Isotherm of $CO_2$ sorption on $Na_2ZrO_3$ at 700 °C. The dashed lines correspond to the data fitting of only short times (double exponential model) or long times (single exponential model). The straight line corresponds to fitting the whole data to a triple exponential model.

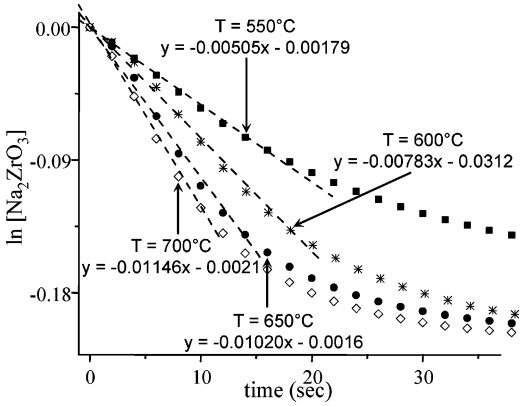


**Figure 10.** Plot of ln[$Na_2ZrO_3$] vs time. The different data present a linear behavior only for short times, which correspond to the times where only the chemisorption process takes place.

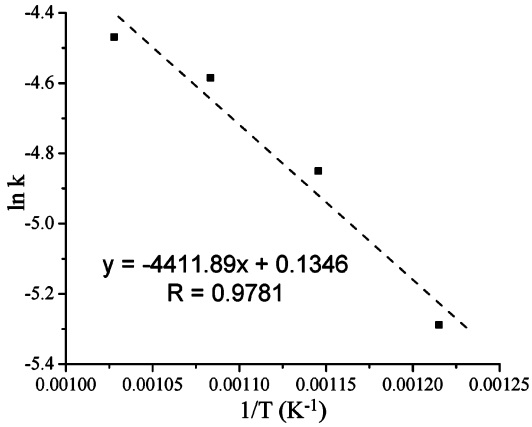


**Figure 11.** Arrhenius-type plot of ln $k$ vs $1/T$, for data obtained assuming a first-order reaction for [$Na_2ZrO_3$].

fact, a further analysis of the isotherm performed at 700 °C showed a desorption process (Figure 9). Therefore, this isotherm showed three different trends. First, at short times, the increment of weight was equal to that observed for the other isotherms, fitting these data to a double exponential model. The $k_1$ and $k_2$ values obtained adjusted the previous analysis very well. Then, the curve showed a lag period, in which the absorption did not increase. Finally, at long times, the desorption process became evident. The sample lost approximately 0.03 wt %. When these data were fitted to a single exponential model, one desorption constant value ($k_3$) equal to $7 \times 10^{-5}$ $s^{-1}$ was obtained. Finally, using the whole data, a different fitting was performed with a triple exponential model, in which the three processes were considered (chemisorption, diffusion, and desorption). In this case, the three constants were similar to the values previously obtained by using simpler models (see Figure 9). Although the desorption constant value obtained was considerably small, it could affect the final $CO_2$ total absorption. In summary, this result strongly suggests that the best $CO_2$ absorption was produced at 600 °C because at higher temperatures, the desorption process occurred, limiting $CO_2$ capture.

A second and totally different way to analyze these isothermal results was proposed to verify the chemisorption energy values obtained previously. In this case, only the high-temperature experiments were used (550−700 °C), to eliminate any influence produced by the sintering effect. Considering that those experiments were carried out into a flux of $CO_2$ in excess, it can be assumed that reaction 1 corresponds to a first-order reaction with respect to $Na_2ZrO_3$, Therefore

$$\ln[Na_2ZrO_3] = -kt \qquad (4)$$

where $k$ is the reaction rate constant, $t$ is the time, and [$Na_2ZrO_3$] is the molar concentration of the ceramic available. Figure 10 shows the plots of ln[$Na_2ZrO_3$] versus time at different temperatures. As expected, the data only followed a straight line at short times, before the $Na_2CO_3$ external shell was completed, and consequently, the diffusion process was activated.

Again, if the $k$ values, obtained from Figure 10, are dependent on temperature, the plot of ln $k$ versus $1/T$ must be a straight line (Figure 11). In this case, the obtained value of the activation energy was 36 680 J/mol, which is a very close value to that obtained by the double exponential model proposed previously (33 866 J/mol). Actually, the difference between the two models is only 8.3%. Furthermore, in this case, only the high-temperature experiments were utilized, while in the other model, all the experimental data were used. Thus, it can be said that both methods agree, and they can be used independently to obtain the activation energy of the chemisorption process. The only condition is that the chemisorption process has to be linearly dependent on temperature.

## Conclusion

$CO_2$ absorption kinetics, of $Na_2ZrO_3$, was analyzed in this work. First, the sample was prepared by a solid-state reaction and then characterized to obtain composition, morphology, particle size, and textural properties (surface area and pore volume).

The isothermal experiments, into a flux of $CO_2$, presented different behaviors depending on the temperature. Between 550 and 700 °C, the $CO_2$ absorption was very fast. On the contrary, between 150 and 300 °C, the $CO_2$ absorption was uncommon. While the isotherm at 150 °C absorbed 17 wt % after 5 h, the sample treated at 200 °C only absorbed 10 wt %. This decrease was more evident at 250 °C, where only 4 wt % was absorbed after the same time. The explanation given to this atypical behavior is associated with a thermal shock produced on the samples during the heating process, which produced a sintering of the powders, and therefore, its surface area decreased as well, inhibiting $CO_2$ absorption.

Although a sintering effect interferes with the $CO_2$ absorption process at low temperatures, all the isotherms were fitted to a double exponential model, to perform a kinetic analysis. The

activation energies for the $CO_2$ absorption and the diffusion of sodium were estimated to be 33 866 and 48 009 J/mol, respectively. Therefore, the sodium diffusion is the limiting step of the total process. Finally, a second analysis was performed to verify the activation energies obtained. In that case, a first-order reaction model was used to determine the $CO_2$ absorption activation energy, obtaining an $E_a$ value of 36 680 J/mol, which confirmed the first value obtained. The best temperature for $CO_2$ absorption on $Na_2ZrO_3$ corresponds to 600 °C. While at lower temperatures sintering and diffusion problems were observed, at higher temperatures, the desorption problem was present, decreasing the efficiency of capture.

**Acknowledgment.** This work was financially supported by the Consejo Nacional de Ciencia y Tecnología (CONACYT) and the Universidad Nacional Autónoma de México (UNAM) through Projects 46522Q-SEP-CONACYT, 23418-SEMARNAT-CONACYT, and IN103506-PAPIIT-UNAM. I.A.-C. thanks CONACYT for financial support (Project 46522Q).

## References and Notes

(1) Kato, M.; Yoshikawa, S.; Nakagawa, K. *J. Mater. Sci. Lett.* **2002**, *21*, 485−487.
(2) Dijkstra, J. W.; Jansen, D. *Energy* **2004**, *29*, 1249−1257.
(3) Wei, X.; Liu, X.; Deeba, M. *Appl. Catal., B* **2005**, *58*, 41−49.
(4) Kwak, M. S.; Hwang, J. S.; Park, C. O.; Miura, N.; Yamazoe, N. *Sens. Actuators, B* **1999**, *56*, 59−64.
(5) Karlsen, E. J.; Nygren, M. A.; Pettersson, G. M. *J. Phys. Chem. B* **2003**, *107*, 7795−7802.
(6) Pannocchia, G.; Puccini, M.; Seggiani, M.; Vitolo, S. *Ind. Eng. Chem. Res.* **2007**, *46*, 6696−6706.
(7) Wirawan, S. K.; Creaser, D. *Microporous Mesoporous Mater.* **2006**, *91*, 196−205.
(8) Ocho-Fernández, E.; Rønning, M.; Grande, T.; Chen, D. *Chem. Mater.* **2006**, *18*, 6037−6046.
(9) Macario, A.; Katovic, A.; Giordano, G.; Iucolano, F.; Caputo, D. *Microporous Mesoporous Mater.* **2005**, *81*, 139−147.
(10) Nomura, K.; Tokumistu, K.; Hayakawa, T.; Homonnay, Z. *J. Radioanal. Nucl. Chem.* **2000**, *246*, 69−77.
(11) Yong, Z.; Rodrigues, A. E. *Energy Convers. Manage.* **2002**, *43*, 1865−1876.
(12) Nakagawa, K.; Ohashi, T. *J. Electrochem. Soc.* **1998**, *145*, 1344−1346.
(13) Mosqueda, H. A.; Vazquez, C.; Bosch, P.; Pfeiffer, H. *Chem. Mater.* **2006**, *18*, 2307−2310.
(14) Pfeiffer, H.; Bosch, P. *Chem. Mater.* **2005**, *17*, 1704−1710.
(15) Venegas, M. J.; Fregoso-Israel, E.; Escamilla, R.; Pfeiffer, H. *Ind. Eng. Chem. Res.* **2007**, *46*, 2407−2412.
(16) Veliz-Enriquez, M. Y.; Gonzalez, G.; Pfeiffer, H. *J. Solid State Chem.* **2007**, *180*, 2485−2492.
(17) Xiong, R.; Ida, J.; Lin, Y. S. *Chem. Eng. Sci.* **2003**, *58*, 4377−4385.
(18) López-Ortiz, A.; Perez-Rivera, N. G.; Reyes-Rojas, A.; Lardizabal-Gutiérrez, D. *Sep. Sci. Technol.* **2004**, *39*, 3559−3572.
(19) Ida, J. I.; Xiong, R.; Lin, Y. S. *Sep. Purif. Technol.* **2004**, *36*, 41−51.
(20) Gauer, C.; Heschel, W. *J. Mater. Sci.* **2006**, *41*, 2405−2409.
(21) Essaki, K.; Kato, M.; Uemoto, H. *J. Mater. Sci.* **2005**, *40*, 5017−5019.
(22) Escobedo-Bretado, M.; Guzmán-Velderrain, V.; Lardizábal-Gutiérrez, D.; Collins-Martínez, V.; Lopez-Ortiz, A. *Catal. Today* **2005**, *107−108*, 863−867.
(23) Essaki, K.; Nakagawa, K.; Kato, M.; Uemoto, H. *J. Chem. Eng. Jpn.* **2004**, *37*, 772−777.
(24) Choi, K. H.; Korai, Y.; Mochida, I. *Chem. Lett.* **2003**, *32*, 924−925.
(25) Zhao, T.; Rønning, M.; Chen, D. *Chem. Mater.* **2007**, *19*, 3294−3301.
(26) Pfeiffer, H.; Lima, E.; Bosch, P. *Chem. Mater.* **2006**, *18*, 2642−2647.
(27) Pfeiffer, H.; Vazquez, C.; Lara, V. H.; Bosch, P. *Chem. Mater.* **2007**, *19*, 922−926.